The clean and hydrated low-index Rb2Ti2O5 surfaces

Guillaume Benas, Sofia de Sousa Coutinho, Brigitte Leridon, Fabio Finocchi

▶ **To cite this version:**

Guillaume Benas, Sofia de Sousa Coutinho, Brigitte Leridon, Fabio Finocchi. The clean and hydrated low-index Rb2Ti2O5 surfaces. Physical Chemistry Chemical Physics, 2025, 27 (18), pp.9537-9548. ⟨10.17172/NOMAD/2024.11.21-1⟩. ⟨hal-05037200⟩

HAL Id: hal-05037200

https://hal.science/hal-05037200v1

Submitted on 16 Apr 2025

HAL is a multi-disciplinary open access archive for the deposit and dissemination of scientific research documents, whether they are published or not. The documents may come from teaching and research institutions in France or abroad, or from public or private research centers.

L'archive ouverte pluridisciplinaire **HAL**, est destinée au dépôt et à la diffusion de documents scientifiques de niveau recherche, publiés ou non, émanant des établissements d'enseignement et de recherche français ou étrangers, des laboratoires publics ou privés.

Distributed under a Creative Commons CC BY-NC 4.0 - Attribution - Non-commercial use - International License

THE CLEAN AND HYDRATED LOW-INDEX $Rb_2Ti_2O_5$ SURFACES

Guillaume Benas
Institut des Nanosciences de Paris, INSP,
Sorbonne Université, CNRS, F-75005 Paris, France.
Laboratoire de Physique et d'Etude des Matériaux, LPEM,
Ecole Supérieure de Physique et Chimie Industrielles,
Université Paris Sciences et Lettres, Sorbonne Université, CNRS, F-75005 Paris, France.
guillaume.benas@insp.jussieu.fr

Sofia De Sousa Coutinho
Laboratoire de Physique et d'Etude des Matériaux,
Ecole Supérieure de Physique et Chimie Industrielles, LPEM,
Université Paris Sciences et Lettres, Sorbonne Université, CNRS, F-75005 Paris, France.
Materials Department, University of Oxford, Oxford, OX1 3PH, UK

Brigitte Leridon
Laboratoire de Physique et d'Etude des Matériaux, LPEM,
Ecole Supérieure de Physique et Chimie Industrielles,
Université Paris Sciences et Lettres - Sorbonne Université, CNRS, F-75005 Paris, France.
Pioniq, 6 rue Jean Calvin -75005 Paris
brigitte.leridon@espci.fr

Fabio Finocchi
Institut des Nanosciences de Paris, INSP,
Sorbonne Université, CNRS, F-75005 Paris, France.
fabio.finocchi@insp.jussieu.fr

Preprint version (18/03/2025) - This article has been peer-reviewed and is currently awaiting for publication in :
Physical Chemistry Chemical Physics.

ABSTRACT

Despite the remarkable dielectric properties of $Rb_2Ti_2O_5$ upon exposure to humid atmosphere, its surfaces are still poorly known, to date. Here we study the atomic-scale structure of the clean (100), (010) and (001) surfaces, and the onset of water adsorption, via Density Functional Theory. Among them, the clean (001) surface has a very low surface energy, much smaller than most terminations of other perovskites or titania. $Rb_2Ti_2O_5$(001) is also very reactive towards water, which adsorbs as a molecule, forming regular water arrays on the surface. From the calculations, we conclude that $Rb_2Ti_2O_5$ could very easily cleave at ambient conditions, forming (001) planes with ordered adsorbed water and almost null surface stress. Although $Rb_2Ti_2O_5$ is a three-dimensional crystal, it behaves in this respect as two-dimensional compounds, such as graphite or layered perovskites.

1 Introduction

Most stoichiometric solid oxides are electronic insulators. Among them, several ones are proton conductors after incorporation of protonic defects, which often follows water absorption. This phenomenon was firstly discovered by

Iwahara in the eighties in Ce-based and Sr-based perovskites [1, 2, 3], thus opening the possibility to use oxide ceramics as electrolyser membranes and more generally for energy storage applications [4].

The research on solid proton conductors actually includes perovskite-derived oxides.[5] However, very few of them show proton conductivities above 1 mS/cm at 300°C, and their conductivity is expected to fall well below at room temperature.[5] One of the key aspects is whether the incorporated water molecule dissociates, resulting in a hydroxyl group and a proton, with the eventual formation of hydrogen bonds with O anions in the solid. Another issue is that proton incorporation does not entail hole creation, yielding undesired electronic conductivity. Understanding the mechanisms for water incorporation or water adsorption on the surface and its possible diffusion into the bulk is therefore of paramount importance in order to identify intrinsic proton-conducting oxides.

$Rb_2Ti_2O_5$ [6] and related materials have recently been identified as solid electrolytes with ionic conductivity larger than 1 mS/cm at room temperature and colossal capacitance when interfaced with metals [7, 6, 8, 9]. As-prepared $Rb_2Ti_2O_5$ crystals appear as transparent lamellar needles typically few nm long [7]. $Rb_2Ti_2O_5$ belongs to the Andersson-Wadsley class of compounds [10, 11]. Its crystal structure remains invariant and centro-symmetric at all temperatures between 90 and 450 K [6]. The material can be easily cleaved parallel to (001) planes. It has been shown that $Rb_2Ti_2O_5$ samples, even when synthesized in water-free environment, can incorporate significant amounts of water (up to 35%) with tiny variations of the lattice parameters and that their electric properties are sensitive to the water content [12, 13]. Recent studies stress the interest of layered titanates for proton incorporation, with particular importance of the interlayer space where water molecules as well as hydronium ions could be found [14]. However, to the best of our knowledge, the surfaces of Andersson-Wadsley compounds are still unexplored, and $Rb_2Ti_2O_5$ makes no exception. In order to partially fill this gap and understand how the surface stability and hydration could influence the properties of the material and the reactivity of the $Rb_2Ti_2O_5$ surfaces to water, as well as a first step to understand water incorporation in the bulk, we compute the structure of low-index, unreconstructed $Rb_2Ti_2O_5$ surfaces and the thermodynamics of water adsorption, via the Density Functional Theory (DFT).

2 Methods

2.1 DFT calculations

The density functional theory calculations were performed using the Quantum ESPRESSO package [15]. The exchange-correlation functional was modeled using the Perdew-Burke-Ernzerhof functional, as revised for solids (PBEsol) [16, 17]. The interaction between ions and valence electrons were described using optimized norm-conserving pseudo-potentials [18]. A minimum energy cutoff of 80 Ry was employed for the plane-wave basis set. We use a k-point $2 \times 6 \times 4$ grid for sampling the bulk Brillouin zone, which is reduced to the sole Γ point along the direction normal to the surface when considering slabs including many atomic layers plus a void space. The calculations were performed by setting the minimum threshold for the convergence of the total energy during the Kohn-Sham cycles at 10^{-8} Ry and at 10^{-3} Ry/a.u. for the largest residual atomic forces after geometry optimization. Other computational details can be found in the Supplemental Material, as well as some tests of the relevance of dispersion interactions using DFT-D3 [19].

2.2 Bulk properties

The ternary titanium oxides denoted by $A_2Ti_nO_{2n+1}$ (A = Li, Na, K, Rb, Cs) are known as the Andersson–Wadsley type alkali titanates with layered structure for $2 \leq n \leq 5$ [10, 11][20]. Some of them present ferroelectric phase transitions, with remarkably high Curie temperatures [21].

$Rb_2Ti_2O_5$ owns C2/m space group (Table 1)and a layered structure, which consists in alternate RbO/Ti_2O_3/RbO plan stacks along the c-axis, as represented in Fig. 1 [10, 6]. The motif includes three non-equivalent oxygen atoms, which we label by the number of covalent bonds they form with Ti atoms: $O^{(1)}$, $O^{(2)}$, and $O^{(3)}$. The Ti_2O_3 layers can be described as dense chains of Ti and $O^{(3)}$ atoms linked together by $O^{(2)}$ atoms, which form the tilted square bases of pyramids with Ti atoms in the centre. These pyramids share edges formed by the $O^{(3)}$ atoms, and share corners at the $O^{(2)}$ atoms positions. The pyramid apex are the oxygen atoms $O^{(1)}$ of the RbO plans, pointing upward or downward. The Ti atoms at the pyramid centres are 5-fold coordinated. The Rb atoms are located in the space between the pyramids, at roughly same positions along c as the $O^{(1)}$ apical ions. Their shortest bonds are with $O^{(2)}$ atoms. The $RbO^{(1)}$ plans are also linked to neighbouring $RbO^{(1)}$ layers through Rb-$O^{(1)}$ bonds along c, which ensures the overall crystal cohesion. The diagonal elastic constants are of the order of the Mbar (Table 2). The zz component is considerably lower than the other two diagonal components, which underlines the layered nature of the crystal along c. By relating the applied pressure to the crystal volume variation, we estimate the bulk modulus $B_0 \simeq 610$ kbar, in good agreement with previous calculations [6].

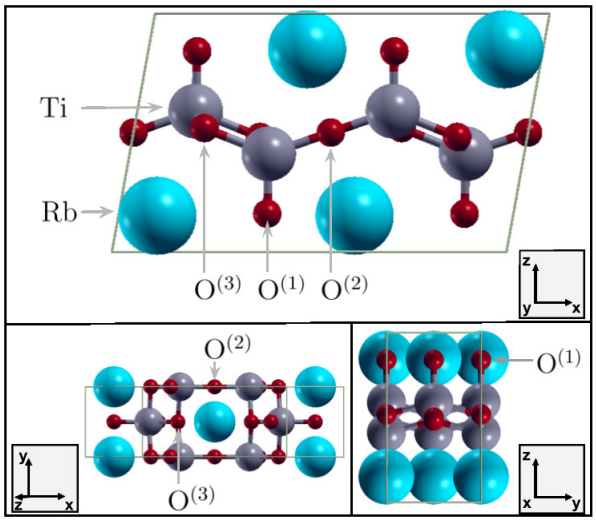

Figure 1: **Primitive $Rb_2Ti_2O_5$ cell** with the crystal axes represented using Xcrysden [22]. Rb in blue, Ti in grey and O in red. $O^{(n)}$ denote O that are n-fold coordinated to Ti (see main text).

Cell parameters	this work	Experimental (T=100K)
a (Å)	11.302	11.343
b (Å)	3.796	3.826
c (Å)	6.947	6.970
β (°)	100.20	100.338
V (Å^3)	293.338	297.521

Table 1: **Computed and measured structural parameters of the $Rb_2Ti_2O_5$ crystal.** V is the unit-cell volume. The experimental values are taken from Ref.[6].

C_{xx}(kbar)	C_{yy} (kbar)	C_{zz} (kbar)	B_0 (kbar)
1182	1392	789	610

Table 2: **Computed diagonal elastic constants and bulk modulus** B_0.

2.3 Surface energy and surface stress

For a crystal, the interface between a surface of Miller index (hkl) and a void region results in the atom relaxation and an excess energy as compared to the bulk. This excess energy is related to the surface energy, which is calculated using the following procedure. First, a bulk supercell with N layers along the surface normal $\hat{n}$ is constructed and its lattice parameters fully relaxed; we denote its energy as $E^{bulk,N}$. Then, we add a void region with minimal thickness of 10 Å, thus obtaining a slab that alternates atomic layers and a void region along $\hat{n}$ (periodic boundary conditions apply parallel and normal to the surface). Few inner layers of the slab are clamped in their bulk positions, while the remaining atoms are relaxed. $E^{slab,N}$ is the corresponding total energy after the slab relaxation. Finally, we compute the surface energy for the slab with N layers as :

$$\gamma_N = \frac{1}{2A_{hkl}}(E^{slab,N} - E^{bulk,N}) \tag{1}$$

with A_{hkl} the surface area. The surface energy of the (virtual) infinite crystal (that is, in the $N \to \infty$ limit) can be computed via a linear regression on slabs with varying N: the intercept provides the surface energy $\gamma_{(hkl)}$, with the corresponding error bar.

As the lateral lattice parameters are kept fixed at their values as obtained in the bulk supercell, the absence (or variation) of neighboring atoms for the outermost layer atoms induces a surface stress [23, 24]. The surface stress tensor $\bar{\sigma}_{ij}$ is defined as the derivative of the surface energy with respect to the strain in the i, j directions parallel to the surface plane [24]. The diagonal components $\bar{\sigma}_{ii}$ can be negative (compressive stress) whenever a dilation along i decreases the surface energy; symmetrically, it is positive (tensile stress) whenever a contraction along i decreases the surface energy.

[1] We evaluate the surface stress in the parallel directions to the surface via the difference of the diagonal components of the stress tensor σ for the N-layer slab and the bulk supercell, as:

$$\bar{\sigma}_{ii}^{(N)} = \frac{1}{2A_{hkl}}(V^{slab,N}\sigma_{ii}^{slab,N} - V^{bulk,N}\sigma_{ii}^{bulk,N}) \tag{2}$$

with $V^{slab,N}$ and $V^{bulk,N}$ the supercell volume for the slab and the bulk calculations, respectively. Then, we perform a linear regression with different N, in order to obtain the surface stress in the limit of an infinite numbers of layers, as for the surface energy.

In section 3, the atomic structure and the surface energy and stress will be analyzed for each termination and related to their atomic structures.

2.4 Stability of the hydrated surface

In this section, we describe how the surface energy upon adsorption of n molecules per unit surface area is evaluated. We focus on the case of water adsorption, although the generalization to other kinds of molecules is straightforward [25]. Firstly, we compute the adsorption enthalpy $\Delta^{(n)}H_{hkl}^{ads}$ of the n ad-molecules by the total energy difference between the hydrated surface on one side, and the clean surface and the isolated molecules on the other side. Here, $\Delta^{(n)}H_{hkl}^{ads}$ refer to the configurations that are obtained after full atomic relaxation, which therefore corresponds to $T = 0$ K and thus neglects temperature effects (quantum contributions, such as the zero-point energy, are also neglected at this stage). Secondly, we assume that the vibrational contributions to the enthalpy are almost the same ones in the solid phases (the clean and wet surfaces); thus, they roughly compensate each other (as well as the zero-point energy). Third, we assume that the main contribution to the entropy comes from rotations and translations of the water molecules in the gas phase, for which the chemical potential per water molecule from translations and rotations $\mu_{\mathrm{H_2O(gas)}}^{(\mathrm{tr+rot})}$ can be evaluated in the ideal gas approximation or taken from tabulated data as a function of T [26]. Finally, the free energy variation upon water adsorption on the (hkl) surface from an ideal gas reservoir is estimated as :

$$\Delta^{(n)}G_{hkl}^{(gas)}(p,T) = \Delta^{(n)}H_{hkl}^{ads} - n\,\mu_{\mathrm{H_2O(gas)}}^{(\mathrm{tr+rot})}(p,T) \tag{3}$$

A configuration is stable if $\Delta^{(n)}G_{hkl}^{(gas)}(p,T) \leq 0$, the equality corresponding to the stability line. From $\Delta^{(n)}G_{hkl}^{(gas)}(p,T) = 0$ one can deduce the minimum partial pressure P_{des} at temperature T at which the actual configuration is stable (or the maximum temperature T_{des} at a given water partial pressure p). Within the ideal gas approximation for the water vapor phase, the critical pressure can be expressed as :

$$P_{des}(T) = \mu^{(rot)}(T)\,\frac{k_B T}{\lambda^3(T)}\,\exp\left(\frac{\Delta^{(n)}H^{ads}}{nk_B T}\right) \tag{4}$$

where $\mu^{(rot)}$ is the purely rotational contribution to the chemical potential of the water molecule (which is independent of p), and λ its de Broglie thermal wavelength, which appears in the translational partition function. Thus for a partial pressure $p < P_{des}(n,T)$ the configuration with n adsorbed molecules per unit surface area is unstable according to thermodynamics.

In the experimental conditions, water is often much closer to the liquid state than to an ideal gas. In order to provide a limiting case which takes into account water molecules cohesion in the reservoir, we choose as reference the ice Ih crystal rather than the liquid and define the free energy variation upon water adsorption on the (hkl) surface from the solid reservoir as :

$$\Delta^{(n)}G_{hkl}^{(ice)}(T) = \Delta^{(n)}H_{hkl}^{ads} - n\,\left(\varepsilon + \mu_{\mathrm{H_2O(ice)}}^{(\mathrm{conf})}(T)\right) \tag{5}$$

where the binding energy per water molecule is $\varepsilon \simeq -0.81$ eV and $\mu_{\mathrm{H_2O(ice)}}^{(\mathrm{conf})}$ includes the configurational entropy in the ice crystal [27, 28]. The stability of the hydrated surface is evaluated via the surface free energy :

$$\Gamma_{hkl}^{(res)}(n,p,T) = \gamma_{hkl} + \Delta^{(n)}G_{hkl}^{(res)}(p,T)/A_{hkl} \tag{6}$$

with respect to the specific reservoir (*res*= gas or ice). For each surface, this quantity will be evaluated using both gas and ice phases, representing the two limiting cases that enclose the energy of the water molecules in the actual reservoir. The stability of hydrated surfaces in relation to the experimental conditions will be discussed in section 4. Here, we remind that both $\Gamma_{hkl}^{(gas)}(n,p,T)$ and $\Gamma_{hkl}^{(ice)}(n,T)$ can be affected by the actual approximations employed for the exchange-correlation functional [29].

[1] Note on units: 1 meV/Å^2 $\simeq$ 16 mJ/m^2.

3 Clean surfaces

For each low-index (100), (010) and (001) terminations, in the following we analyze the surface energy, the surface stress and the atomic relaxations as obtained by full optimization. In the absence of any experimental indication on possible surface reconstructions, we consider only unreconstructed terminations, corresponding to (1×1) surface unit cells.

3.1 The (100) surface

Cleaving $Rb_2Ti_2O_5$ to form the (100) surface requires a special care [30]. Along the surface normal, there is a $RbTiO_2$/O/$RbTiO_2$ stack: the $RbTiO_2$ planes with +1 formal charge, contain both $O^{(1)}$ and $O^{(3)}$ ions, while the oxygen plane with -2 formal charge is formed by $O^{(2)}$ ions (see Fig. 2). The $RbTiO_2$/O/$RbTiO_2$ stack corresponds to a neutral, stoichiometric unit with no dipole along the the surface normal. Accordingly, the $RbTiO_2$/O/$RbTiO_2$ termination is a type-II polar surface [31, 32]. The dipole-free and stoichiometric (100) surface, as terminated by $RbTiO^{(1)}O^{(3)}$ planes, is symmetric with respect to the central $O^{(2)}$ layer. Despite the fact that the cleaving process breaks a large number of bonds the estimated surface energy $\gamma_{(100)} \simeq 45.0$ meV/Å^2 is about the same order as for the other low-index surfaces (see Tab.3).

Upon full surface relaxation, the surface Ti atoms are 4-fold coordinated to oxygen and their bond lengths with $O^{(2)}$ atoms slightly decrease (Fig.2). The $O^{(3)}$ atoms reduce their coordination number with Ti to 2, which involves less stable electronic states than in the bulk (see Supplementary Materials). Accordingly, surface $O^{(3)}$ atoms move to form a tilted tetrahedron with the other oxygen atoms around the surface Ti. As for Rb at the outermost layer, the bonds with the $O^{(1)}$ atoms and the sub-layer Rb cations contract strongly (red crosses in right panel of Fig.2), which contributes to the relaxation between the surface and sub-surface planes. Interestingly, one can see in the same figure that some of the bond lengths of Rb with the $O^{(2)}$ atoms reduce, while others stretch. Going deeper into the bulk, the bond lengths between the cations (Rb, Ti) and the O anions readily converge to their bulk values within 1% after the second unit block, which shows that the structural rearrangements is essentially restricted to the three outermost layers.

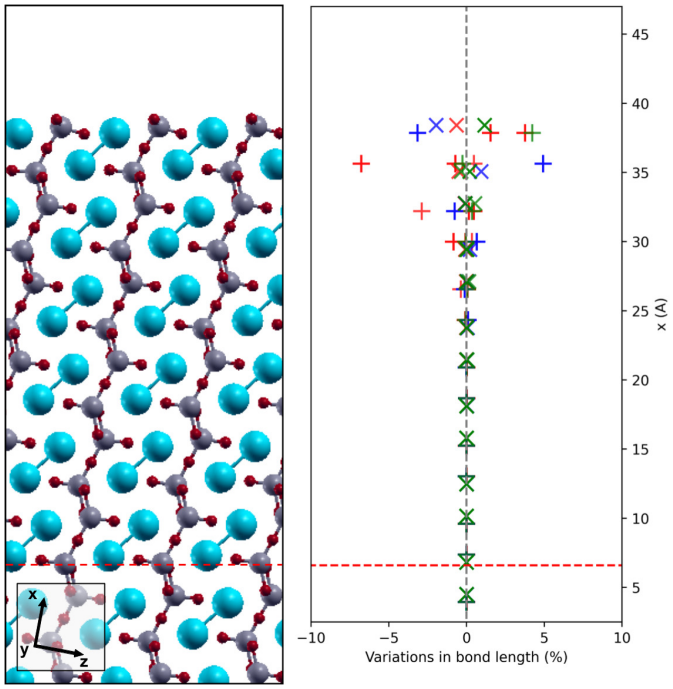

Figure 2: Left panel : representation of the (100) relaxed surface using Xcrysden [22], going from the surface into the bulk along the surface normal. The region beneath the dashed red line corresponds to the bulk region, where the atoms are clamped in their bulk positions. Rb atoms are blue, Ti grey and O red. Right panel : Bond length relative variations with respect to their bulk values, for the layers as drawn in the left panel. The symbol "+" is relative to Rb cations, while the symbol "×" relates to Ti cations. Red symbols correspond to bonds with $O^{(1)}$, blue ones to bonds with $O^{(2)}$ and green ones to bonds with $O^{(3)}$.

As shown in tab.3, the (100) surface presents a relatively low surface stress in the z direction, along which most relaxations described above occur. However, it exhibits a huge tensile (positive) surface stress along the y-axis, which might drive a surface reconstruction or be at the root of enhanced reactivity with adsorbing species. This could be due to the partial rupture of the Ti-$O^{(3)}$ chains at the surface, which cannot easily contract along y without breaking the bulk periodicity in this direction. However, the study of possible surface reconstructions is beyond the scope of the present paper, especially in the absence of detailed experimental studies.

3.2 The (010) surface

The non-polar (010) surface consists in a compact stacking of $Rb_2Ti_2O_5$ layers, of same composition as the bulk (Fig. 3, left panel). The atomic relaxation are reported in the right panel of Fig. 3 as a function of the atom distance from the surface. An $O^{(3)}$ out of three is missing around the surface Ti. This implies the reduction of coordination numbers: the surface Ti atom is 4-fold coordinated (with respect to 5-fold bulk Ti) and the outermost $O^{(3)}$ has only two bonds with Ti, leading to a significant strengthening of the remaining bonds (green cross in Fig.3, right panel). Consistently with the bond shortening, the Ti-$O^{(2)}$-Ti arrangement, which is linear in the bulk, is strongly bent at the surface. The Rb atom, which looses a neighbouring $O^{(2)}$ atom, breaks its quasi-symmetrical position, that is midway between the $O^{(1)}$ atoms in the bulk, thus forming a short bond and a longer one (red crosses in Fig.3, right panel). In the fully optimized slab, the outermost layer experiences a significant inward relaxation, whereas the third one slightly increases its distance from the layer below. Both interatomic distances and layer mean positions along the surface normal converge to their corresponding bulk values after three layers beneath the surface. The reduction of the ionic coordination number and the bond lengths at the surface has consequences on the electronic structure, as detailed in the Supplementary Materials.

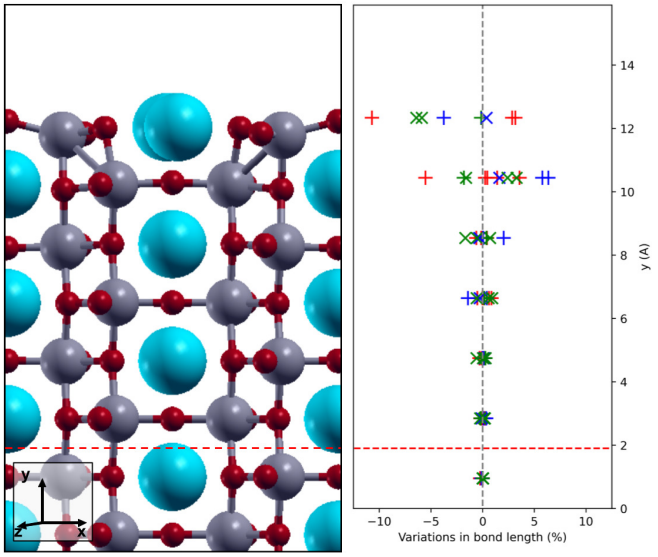

Figure 3: Left panel : representation of the (010) relaxed surface using Xcrysden [22]. Right panel : structural variations relative to the bulk represented according to their distance from the surface. Same conventions as in Fig 2

The computed (010) surface energy $\gamma_{(010)} \simeq 34.8$ meV/Å^2 is quite small as compared to other non-polar terminations of oxide crystals [33], as well as its unsaturated coordination index [34]. Therefore, we predict that the $Rb_2Ti_2O_5$(010) stoichiometric surface could be quite stable. However, the computed surfaces stresses in Tab.3 indicate a relatively strong tendency of the (010) surface to contract in the a-axis direction, as the tensile surface stress in this direction is roughly twice as large as the surface energy. This suggests that the (010) surface might be prone to surface reconstructions or to the formation of extended surface defects.

3.3 The (001) surface

The atomic (001) plans are either formed by RbO (with -1 formal charge) or Ti_2O_3 (with +2 formal charge). The stacking unit consists of RbO / Ti_2O_3 / RbO, which is symmetric with respect to the central Ti_2O_3 layer. The surface can thus be defined as a type-II polar surface [31, 32]. From electrostatic stability arguments, the most stable termination for the stoichiometric (001) surface is RbO : the surface can be thus view as a stacking of neutral and dipole-free units.

Experimentally [6, 35], $Rb_2Ti_2O_5$ cleaves along the (001) surface. Indeed, the formation of the (001) surface can be viewed as an exfoliation of the crystal between two stacking units, which breaks only rather weak bonds between RbO plans. The computed (001) surface energy is very low and amounts to $\gamma_{(001)} \simeq 18.3$ meV/Å^2 (see Tab.3). Such a low surface energy is consistent with the picture of $Rb_2Ti_2O_5$ as a quasi two dimensional material along the surface normal, which is consistent with the very minor changes in the surface electronic structure with respect to the bulk (see Supplementary Materials).

As shown in Fig.4, the Rb outermost atoms slightly strengthen their bonds with the underlying Ti_2O_3 plane. However, the most striking feature is a lateral relaxation of the outermost Rb cations, which leave their quasi-symmetrical position between the apical oxygen $O^{(1)}$ atoms to form a very short bond (2.79 Å instead of 3.14 Å in the bulk). The Rb lateral relaxation is accompanied by the increase of the angle formed by the surface $O^{(1)}$ atoms with the Ti_2O_3 layer underneath. This leads to the creation of a significant space between the Rb atoms and the next row of apical $O^{(1)}$ atoms, which plays a role in the insertion of water and, possibly, other molecules, as we will discuss in the next chapter. Beside that huge surface Rb relaxation, the other atoms are very close to their bulk positions. Indeed, as shown in Fig.4, the Ti-O inter-atomic distances on the layer beneath contract slightly (by about 2%) while the other bond lengths are essentially unchanged with respect to their bulk values. The surface stress along the [100] direction is tensile and of the same magnitude as the surface energy, while it is compressive (negative) along [010], with absolute value larger than the surface energy.

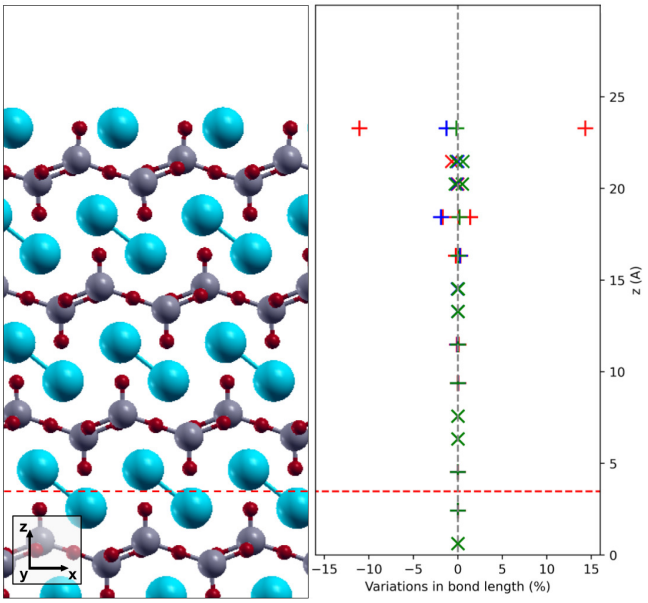

Figure 4: Left panel : representation of the (001) relaxed surface using Xcrysden [22]. Right panel : structural variations relative to the bulk represented according to their distance from the surface. Same conventions as in Fig 2.

3.4 Comparison and Discussion

Our estimates for the surface energy and stress of the three low-index clean surfaces are collected in Tab.3. First, we remark that the surface energy is very low for $Rb_2Ti_2O_5$ (001), as compared to other oxide surfaces [34]. This is consistent with the fact that $Rb_2Ti_2O_5$ naturally cleaves along (001) plans. The (100) surface has the highest surface energy and thus is the less stable one among the three low-index $Rb_2Ti_2O_5$ stoichiometric terminations. Although the surface energy can vary as much as $\sim 20\%$ with the actual exchange-correlation approximation E_{XC} to the DFT [29], the ratio between the surface energies of the distinct terminations is less sensitive to the choice of E_{XC}. The inclusion of dispersion interactions tends to increase slightly the surface energies, as shown in the Supplementary Materials.

The surface stress components are mostly positive (tensile stress) apart from the (001) surface, which exhibits a moderate compressive stress along [010]. The largest absolute surface stress is tensile and occurs on the (100) surface along the [010] direction, which might potentially drive reconstructions of the clean surface so to increase the number of bonds [36].

	γ	$\bar{\sigma}_{xx}$	$\bar{\sigma}_{yy}$	$\bar{\sigma}_{zz}$
(100)	45.0		317.0	23.6
(010)	34.8	64.7		-9.0
(001)	18.3	13.6	-31.3	

Table 3: Computed surface energy γ and surface stress $\bar{\sigma}$ along x, y and z directions of low-index clean surfaces. Units are meV/Å^2.

We computed the relative surface areas in a clean $Rb_2Ti_2O_5$ crystallite at equilibrium by using the Wulff relation $\gamma_{(ijk)}A_{(ijk)} = \text{cont.}$ obtaining : $A_{(100)} = 0.40\ \text{nm}^2,\ A_{(010)} \simeq 0.52\ \text{nm}^2,\ A_{(001)} \simeq 1\ \text{nm}^2$. The (001) surface dominates over the other orientations, yielding a slightly distorted orthorhombic nanocrystals, which is elongated along **c**. Actually, other orientations beyond the three low-index surfaces might appear in the Wulff construction, yielding a more rounded shape for the crystallites at equilibrium. Moreover, we take into account neither surface reconstructions (which might likely reduce $\gamma_{(100)}$ and $\gamma_{(010)}$), nor the effect of surface hydration, which will be discussed in the following sections and might be present in the crystals that grow at ambient conditions.

4 Hydrated surfaces

As the observed properties of $Rb_2Ti_2O_5$ are correlated with the presence of water [12], it is essential to characterize how its surfaces interact with water molecules. We determine the stability of the hydration process via the computed enthalpy $\Delta^{(n)}H^{ads}_{hkl}$ of the reaction where n water molecules are taken from a reservoir (either the ideal gas or the hexagonal ice) and adsorb on the $Rb_2Ti_2O_5(hkl)$ surface:

$$Rb_2Ti_2O_5\ (hkl) + n\ H_2O^{(res)} \longrightarrow (H_2O)_n : Rb_2Ti_2O_5\ (hkl) \tag{7}$$

For each surface, a slab with a thick enough portion of void space (in order to avoid spurious interactions between the ad-molecule periodic images) and a larger unit cell than the (1×1) is firstly used to search for the preferred adsorption sites for a single water molecule per unit surface area. Once the possible isolated adsorption sites have been identified, a slab with smaller surface area is used to characterize configurations with higher densities of ad-molecules.

The definition of a water monolayer can be very tricky in some cases, depending on the actual surface termination. From a pragmatic point of view, we look for the largest number of adsorbed water molecules m_{ad} that form at least a bond with the atoms on the clean surface. This number defines the full monolayer: other water molecules beyond m_{ad} can bind to other water molecules but not to the atoms on the dry surface. We consider fully optimized configurations, so that dynamical fluctuations are not taken into account. Clearly, m_{ad} varies with the termination and the actual surface configuration.

In the following, we consider the configurations that are comparatively stable and minimize the surface stress, which are of particular interest. These configurations will be analyzed, highlighting the trends that may lead to the stabilization of the water-covered surface. Next, after characterizing the adsorption configurations at varying density, the stability of the hydration process will be discussed by relying upon the hydrated surface free energies as defined in the equation 6, in relation to the choice of the water reservoir and to the experimental conditions such as the temperature.

4.1 The (100) hydrated surface

The isolated water molecule. We start from the adsorption of an isolated water molecule, for which we found several adsorption sites as shown in the top panel of Fig. 5, where the water adsorption enthalpy and the bond lengths of the water ad-molecule are shown.

In the most stable configuration ($\Delta^{(1)}H^{ads}_{100} = -1.56$ eV), the isolated water molecule dissociates. The $O^{(w)}H$ group binds to a surface Ti, while the dissociated proton binds to a surface $O^{(3)}$ oxygen atom. The latter atom strongly strengthens its bond with a neighbouring Ti atom (see top left panel in Fig.5). Consequently, the $O^{(3)}$ leaves its symmetrical position between two Ti along y as observed on the clean surface. Water dissociation (Fig.5, top right) eventually leads to a configuration with two almost equivalent Ti-OH arrangements at the termination, except that the $O^{(3)}H$ group donates a short H-bond (1.54 Å) to the $O^{(w)}H$ group (see lower panel of Fig. 5). According to the simulations, the dissociation of the water ad-molecule has no barrier.

In all other metastable adsorption configurations, the water molecule does not dissociate. The $O^{(w)}$ binds to surface Rb atoms, and the protons form H-bonds with the surface oxygen atoms (see lower panel in Fig.5). All of the molecular configurations are at least about 1 eV less stable than the dissociated configuration, which results in the formation

of two hydroxyl groups. We point out that water dissociation results in the stabilization of the $O^{(3)}$ electronic states, much more than for the metastable molecular adsorption configurations (see Supplementary Materials). This result is consistent with the expected high reactivity of the clean unreconstructed (100) surface, as discussed in Sec. 3.4.

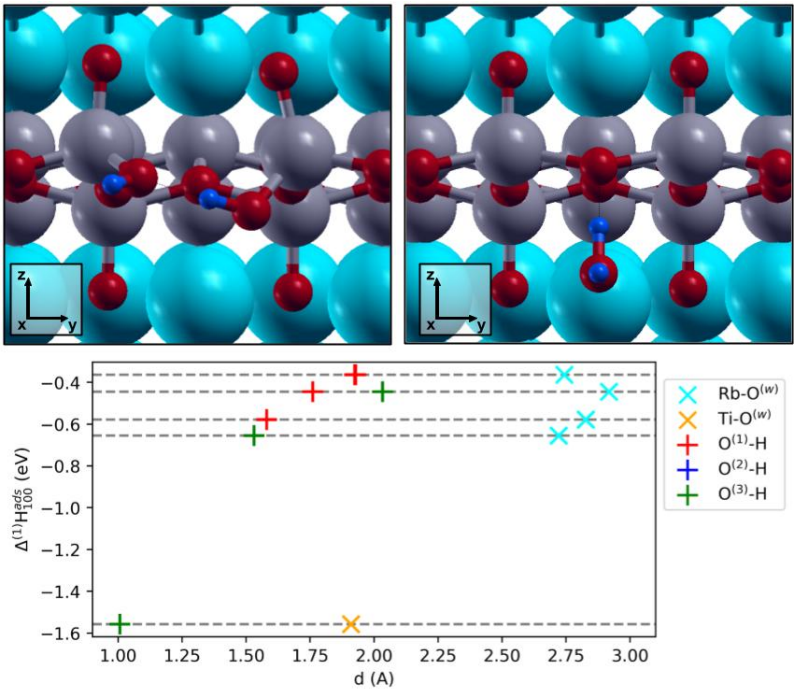

Figure 5: The top panel exhibits the two most stable configurations of a single water molecule on the (100) surface (the most stable dissociated configuration on the left and the second most stable molecular configuration on the right) using XCrysden[22]. The lower panel shows all the identified isolated adsorption sites represented according to their adsorption enthalpy and the relevant bond lengths. Bonds between surface cations and $O^{(w)}$ are represented by '$\times$' crosses : Rb in turquoise and Ti yellow. The bond lengths between the protons and the surface oxygen ($O^{(1)}$ in red, $O^{(2)}$ in green and $O^{(3)}$ in blue) are displayed by '$+$' crosses.

Increasing the water coverage. At higher water coverage on the (100) surface, the most stable configuration ($\Delta^{(1)}H^{ads}_{100} \simeq -1.1$ eV/molecule) involves two dissociated water ad-molecules, in the same fashion as the adsorption of a single molecule. In this case the outermost Ti-$O^{(3)}$ chains along y are fully hydroxylated, which preserves the symmetric position of the $O^{(3)}$ atoms between the Ti and results in the bonding of the $O^{(w)}$ oxygen atoms with the surface Rb atoms. As shown in the top panel of Fig.7, the Rb bonds with the sub-layer $O^{(1)}$ atoms and with the $O^{(3)}$ atoms weaken, as the latter ones bind to protons. As one can see in the lower panel of Fig.7, this configuration leads to a significant relaxation of the surface stress components : $\bar{\sigma}_{yy} = 13$ meV/Å^2 and $\bar{\sigma}_{zz} = -5$ meV/Å^2. The second water molecule adsorbs on the (100) surface as illustrated in Fig.6, forming a H-bond with the apical oxygen as well as two equivalent bonds with Rb atoms at the termination. The corresponding mean adsorption enthalpy is less negative than for the isolated molecule, and the surface stress is slightly negative (see Fig.7). We point out that $m_{ad} = 2$ defines the number of water molecules per unit (100) surface within the monolayer, given that an increase in coverage only leads to molecules binding with previous water ad-molecules.

4.2 The (010) hydrated surface

The isolated water molecule. Several adsorption sites are found for the (010) surface. The adsorption configurations involve bonds between the oxygen atom of the water molecule $O^{(w)}$ and Ti or Rb surface atoms; the hydrogen atoms form H bonds or point out of the surface plan. The most stable configuration for the isolated water molecule corresponds to a negative $\Delta^{(1)}H^{ads}_{010} = -0.91$ eV adsorption enthalpy. The two most stable configurations are reported in Fig. 8. Both structures display Rb-$O^{(w)}$ bonds. The first one (Fig.8, top left panel) consists in a water molecule linking two Ti-$O^{(3)}$ chains through H-bonds in the same fashion as the $O^{(2)}$ atom. In the other configuration (Fig.8, top right panel) $O^{(w)}$ aligns with the bulk apical oxygen atoms $O^{(1)}$, donating a single H-bond to $O^{(3)}$ while the other proton points

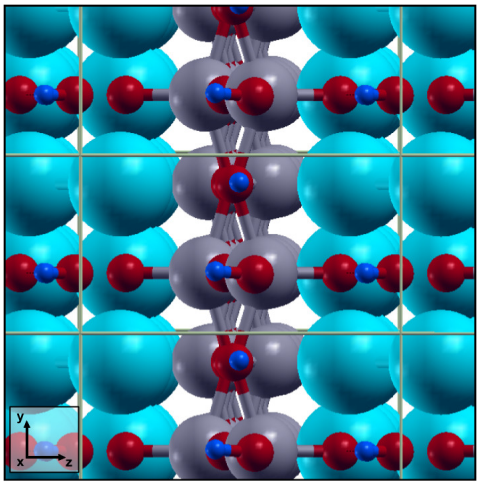

Figure 6: Full monolayer with 2 molecules on the (100) unit surface area (the grey lines represent the cell boundaries) represented using XCrysDen[22].

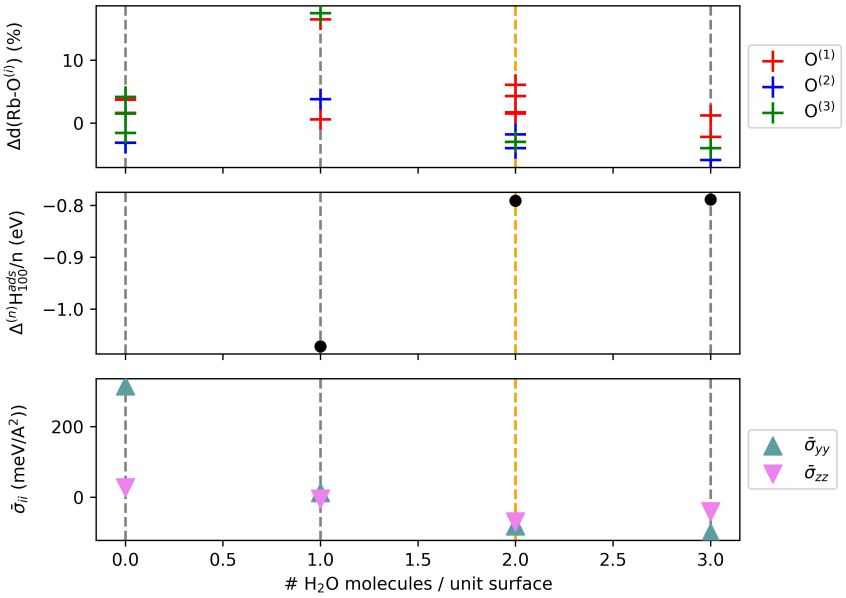

Figure 7: **Coverage of the unit (100) surface.** For different number of water molecules per unit (100) surface, one can see the relative length variations Δ d(Rb-O$^{(i)}$) of the bonds between rubidium and oxygen atoms compared to the bulk values (top panel), the adsorption enthalpy per water molecule $\Delta^{(n)}H^{ads}_{100}/n$ (middle panel) and the surface stress components $\bar{\sigma}_{ii}$ (lower panel). The vertical dashed line colored in orange represents the number of water molecules per unit surface m_{ad} defining the full monolayer.

upward. The latter configuration corresponds to the most stable adsorption site (Fig. 8, lower panel). It exhibits the shortest (and strongest) H-bonds formed with the outermost O$^{(3)}$ atoms, which are highly reactive, consistently with their reduced coordination number at the surface (two instead of three). We point out that there are two such sites per (010) unit surface area. In other metastable adsorption configurations, the water molecule dissociates, with the dissociated hydrogen binding to a surface O$^{(2)}$ atom, while the remaining O$^{(w)}$H group forms a strong bond with a Ti atom (see Supplementary Materials for details).

Increasing the water coverage. The high reactivity of the (010) surface results in a diversity of adsorption sites, indicating that there are multiple ways in which complete hydration can be achieved. A natural way to proceed is to progressively hydrate the surface by selecting one after the other the computed (meta)stable adsorption sites for

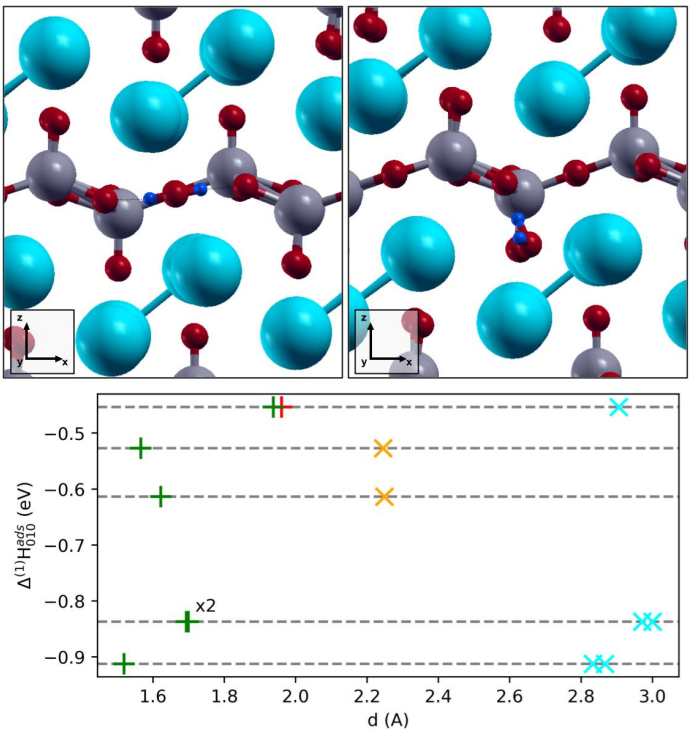

Figure 8: The top panel exhibits the two most stable adsorption configurations of a single water molecule on the (010) surface (on the left, the second most stable configuration, on the right the most stable one) using XCrysDen[22]. The lower panel shows all the identified isolated adsorption sites represented according to their adsorption enthalpy and the length of their bonds with the structure. Bonds between surface cations and $O^{(w)}$ represented with '$\times$' crosses : Rb in turquoise and Ti yellow. Bonds between surface oxygen atoms and water molecule's hydrogen atoms represented with '$+$' crosses : $O^{(1)}$, $O^{(2)}$ and $O^{(3)}$ in red, green and blue, respectively.

the single water molecule. This process is illustrated in Fig.9. In general, the (meta)stable sites for water adsorption coincide with sites in which $O^{(w)}$ occupies the bulk-like O sites that are left empty when $Rb_2Ti_2O_5$ is cut parallel to (010). For instance, $O^{(w)}$ can occupy the lacking $O^{(1)}$ sites, thus restoring the 5-fold Ti coordination as in the bulk.

The full surface hydration as displayed in Fig.9 involves the formation of strong bonds between the $O^{(w)}$ in the water molecules and the outermost Ti atoms at the surface. The water molecules also form H-bonds with the surface oxygen as well as with other ad-molecules, leading to distinct configurations that are almost degenerate in energy. Therefore, we guess that thermal effects could act to mix up all those configurations, although we do not perform long molecular dynamics runs as needed to obtain a full statistics of water adsorption at finite temperatures.

As for the $T = 0$ K most stable configuration for $n = 7$ ad-molecules, we can observe in Fig.9 that all of the H_2O molecules bind to the surface and are located in symmetrical positions with respect to the centre of the two-dimensional unit cell, although they may be engaged in different bonds with the structure and neighbouring water molecules. The most stable hydration configuration as shown in Fig.9 maximizes the number of bonds with the structure as well as between the water molecules. It results in stabilized orbitals for the oxygen atoms of the surface, as well as low-energy states for the adsorbed water molecules (see Supplementary Materials). The outermost Rb atoms bind to the layer of water ad-molecules and therefore strongly relax outwards (see Figure 10). The surface normal through the two-dimensional unit cell is a two-fold rotational axis, which minimizes the total dipole parallel to the surface. Water adsorption also reduces the tensile stress of the clean surface sensitively, which amounts to $\bar{\sigma}_{xx} = -40.5$ meV/Å^2 and $\bar{\sigma}_{zz} = 2.3$ meV/Å^2 for this configuration. Obviously, thermal effects might alter this picture. Nevertheless, given its symmetry and high overall stability, the configuration in Fig.9 will be considered as the reference for the uniformly hydrated (010) surface.

$m_{ad} > 7$ water ad-molecules result in a non-symmetrical arrangement on the (010) surface unit cell and a weak bonding to the surface cations: therefore, we define the $n = 7$ case as the water monolayer. Additional molecules can form very weak bonds with the surface and H-bonds with the other water molecules. Although thermal effects may modify

the atom arrangements, given the many distinct (and almost degenerate) configurations, the critical number of water molecules in the adsorbed monolayer should possibly not exceed $m_{ad} = 7$.

Overall, the hydration process results in dense and complex arrangements of water molecules which compensate for the reduced coordination numbers of the lacking atoms at the surface. Interesting processes such as hydroxylation of the surface via dissociation of a water molecule are likely to occur and could be enhanced by the interactions with the environment. The impact of thermal effects on this water coverage and on the likely creation of radicals would demand a more in-depth study using first-principle molecular dynamics.

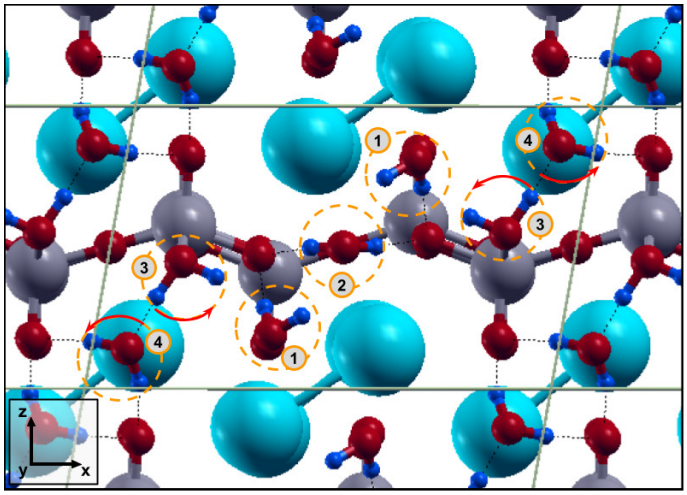

Figure 9: Full monolayer with 7 H_2O molecules on the (010) unit surface area (the gray lines represent the cell boundaries) represented using XCrysDen. [22] The orange circles and associated numbers represent the order in which the sites have been filled, while the red arrows represent possible rotations of the water molecules that could lead to other metastable states.

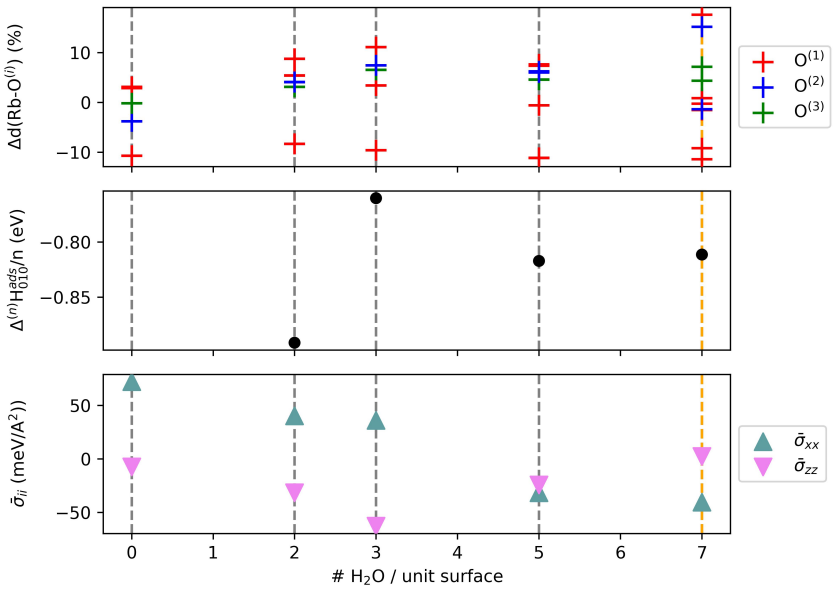

Figure 10: **Coverage of the (010) surface.** For different number of water molecules per unit (010) surface, one can see the relative length variations Δ d(Rb-O$^{(i)}$) of the bonds between rubidium and oxygen atoms compared to the bulk values (top panel), the adsorption enthalpy per water molecule $\Delta^{(n)}H^{ads}_{010}/n$ (middle panel) and the surface stress components $\bar{\sigma}_{ii}$ (lower panel). The vertical dashed line colored in orange represents the number of water molecules per unit surface m_{ad} defining the full monolayer.

4.3 The (001) hydrated surface

The isolated water molecule. The isolated molecule on the (001) surface has a very stable adsorption configuration. The computed enthalpy of adsorption is $\Delta^{(1)}H^{ads}_{001} \simeq -1.23$ eV. The water molecule is incorporated at the termination in the gap left by the Rb atoms that relax toward the apical oxygen atoms $O^{(1)}$ (see Fig. 11). Water adsorption is an exothermic process that strongly stabilizes the (001) surface, regardless of which reservoir (either the ideal water gas or the hexagonal ice crystal) is considered. $H_2O^{(w)}$ forms two strong hydrogen bonds 1.7 Å as long with the surface $O^{(1)}$ ions and two bonds 2.9 Å as long with the surface Rb cations.

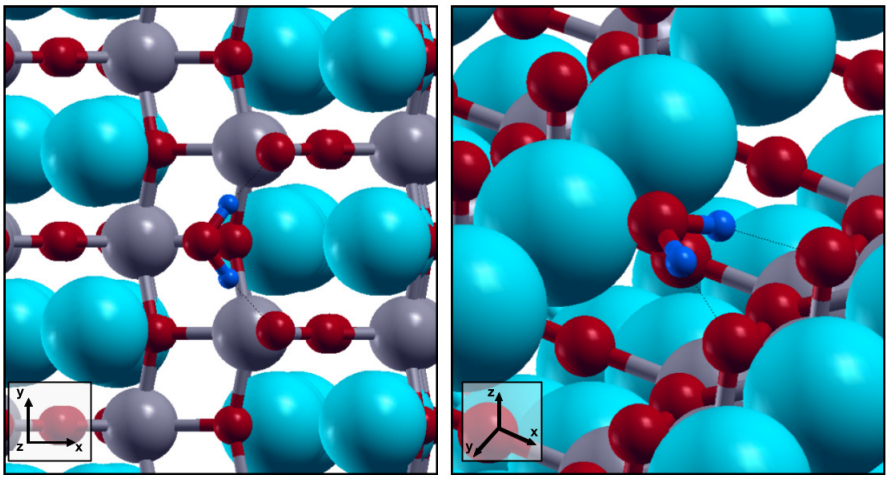

Figure 11: Adsorption site of a single water molecule on the (001) surface represented using XCrysden[22].

Increasing the water coverage. A higher degree of coverage can be obtained by considering the adsorption on two similar sites on the (001) unit two-dimensional cell. The molecules arrange in rows along y, forming strong hydrogen bonds with the apical $O^{(1)}$ and ionic bonds to surface Rb (Fig.12). This results in a quasi one-dimensional alignment of water molecules, which fill the space between the apical $O^{(1)}$ and the surface Rb ions, that eventually results in a well ordered and stable structure at higher coverage. Fig.13 shows the relevant relaxations of the surface in the presence of the water molecules. We point out that the Rb-$O^{(1)}$ bonds are practically unaltered with respect to the clean surface. However, because of the strong Rb-$O^{(w)}$ bonds, the distance between the outermost Rb ions and the underlying Ti_2O_3 plane increases considerably (see Fig.13). All those facts conspire to indicate that the RbO termination of the $Rb_2Ti_2O_5$(001) surface is highly hygroscopic. Water can adsorb in an ordered fashion above each surface Rb via a exothermic process, which results in the formation of a RbO(H_2O) layer with minor structural modifications with respect to the dry surface when other bonds are concerned. Upon hydration, the surface stress along [100] becomes negative (compressive) and of the same order of that along [010].

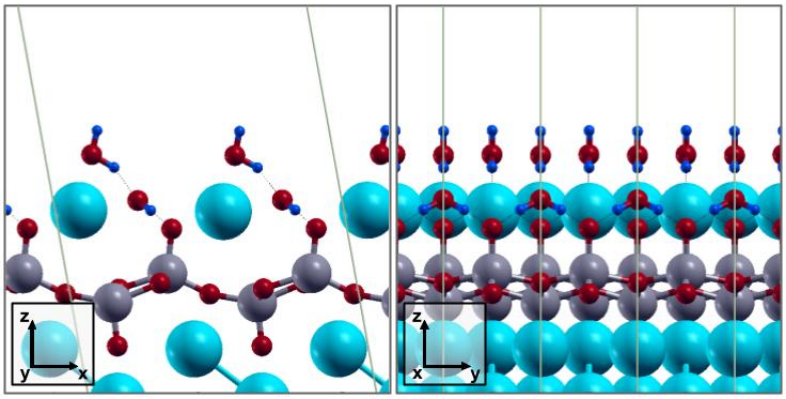

Figure 12: Full monolayer with 4 H_2O molecules on the (001) unit surface area (the gray lines represent the cell boundaries) represented using XCrysDen[22].

As for the next hydration step, the water molecules adsorb above the RbO(H_2O) layer (see Fig.12). The $O^{(w)}$ of the second water molecule sits above the surface Rb; a proton points toward the $O^{(w)}$ ion of the water molecule within the RbO(H_2O) layer, forming a strong hydrogen bond. The other H points outward the surface, forming a small angle with the surface normal. The most striking structural effect is the considerable outward relaxation of the surface Rb ions from the Ti_2O_3 plane beneath, which is due to the interactions with the adsorbed water molecules. Correspondingly, the surface stress is significantly reduced.

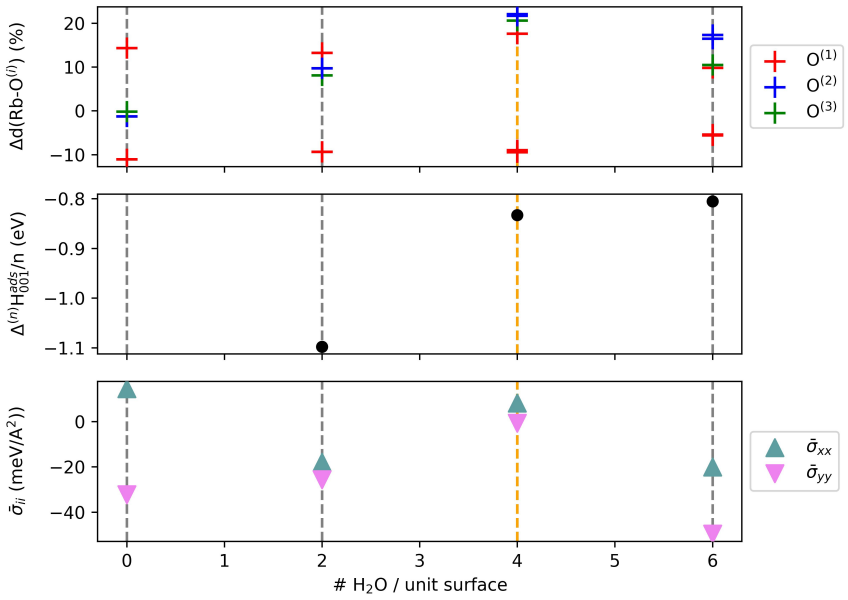

Figure 13: **Bond lengths, adsorption enthalpy and surface stress as a function of the number of water adsorbed molecules on the (001) surface.** Upper panel: Relative length variations Δ d(Rb-$O^{(i)}$) of the bond length between surface Rb and O atoms as compared to the bulk values. Middle panel: the adsorption enthalpy per water molecules $\Delta^{(n)}H^{ads}_{001}/n$. Lower panel: the surface stress components $\bar{\sigma}_{ii}$ (lower panel). The vertical orange dashed line represents the number of water molecules per unit surface $m_{ad} = 4$ defining the full monolayer.

The hydrated surface as represented in Fig. 12 represents the case of the full water monolayer; it displays as a relaxed H_2O/RbO(H_2O) bilayer on the (001) clean surface. Indeed, additional water molecules beyond the H_2O/RbO(H_2O) bilayer will only interact with the molecules already in place rather than with the surface ions. As a consequence of the water-water interaction, the water molecules in the outermost layer weaken their bonds with the surface in order to form hydrogen bonds with the additional water molecules. As shown in Fig.13, this process results in a large reduction of the relaxations observed for the clean surface and for the previous hydration stages. With respect to the clean (001) termination, which displays a compressive stress along y, the configuration with the full water monolayer corresponding to $m_{ad} = 4$ (Fig.12) is at the same time very stable and with a very small surface stress (see lower panel in Fig.13). This suggests that upon increasing surface hydration, the water molecules interact with each other to the point of lessening their interactions with the mono-hydrated surface consisting of a RbO(H_2O) layer, with small binding variation with respect to the bulk material. Further hydration (up to the formation of an interface between the hydrated RbO(H_2O) layer and liquid water) might also result in the Rb solvation and/or formation of RbOH layers, consistently with the experimental observations [35]. However, long molecular dynamics simulations with specific sampling techniques [37] would be needed to that aim, which is outside the scope of the present work.

4.4 Trends in water adsorption on the $Rb_2Ti_2O_5$ surfaces

For each low-index surface, the stability line (see its definition in Sec. 2.4) of the most stable adsorption configurations for the isolated molecule as well as the full water monolayer are represented in Fig. 14. As expected, the desorption temperature increases with the partial pressure of the vapor ideal gas. All hydrated configurations are stable towards sublimation at the room temperature T$\sim$300K even for water partial pressures as low as 10^{-8} atm.

Overall, water adsorption is a strongly exothermic process on all the low-index surface terminations. The adsorption enthalpy for the isolated water molecule on the surface is $\Delta^{(1)}H^{ads}_{100} = -1.56$ eV, $\Delta^{(1)}H^{ads}_{010} = -0.91$ eV and

$\Delta^{(1)}H^{ads}_{001} = -1.23$ eV, on the (100), (010) and (001) surfaces, respectively. These values compare to the water adsorption enthalpy on low-coordinated sites, such as step edges on other oxide surfaces [38, 39] and show the very high reactivity of $Rb_2Ti_2O_5$ towards water. In passing, we note that the computed water adsorption enthalpy is more negative for the isolated water molecule than for the full monolayer (see Fig.14), despite the formation of strong hydrogen bonds within the adsorbed water molecules that occur on all of the surfaces we investigated. This effect is mainly due to the presence of several distinct adsorption sites, the most stable of which are initially saturated. Therefore, the water adsorption enthalpy of the full water mono-layer roughly corresponds to an average among all of the available (meta)stable surface sites.

The (100) surface is particularly reactive and the water molecule dissociates without kinetic barriers. It displays the most negative water adsorption enthalpy (see Sec. 4.1), both for the isolated molecule and the full water monolayer. Accordingly, water sublimation could occur at much higher temperatures than the ambient one for a water partial pressure of 10^{-2} atm. The water molecule on the (001) surface is the second most stable one and could desorb at $T \sim 500$ K for $p \sim 10^{-2}$ atm.

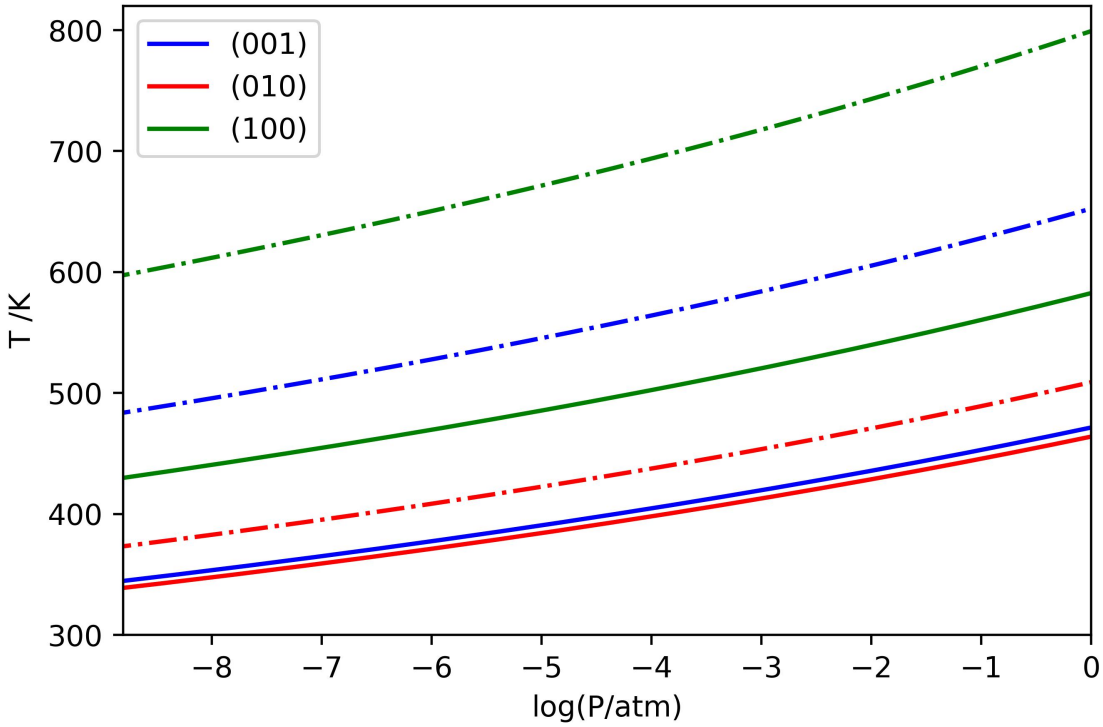

Figure 14: Stability lines ($\Delta G^{(gas)}_{hkl}(n, p, T) = 0$, see Sec.2.4) corresponding to the isolated water molecule (dot-dashed lines) and the full water monolayer (full lines) for the three low-index $Rb_2Ti_2O_5$ surfaces.

Also significant is the surface free energy with respect to a virtual ice reservoir, which is, below room temperature, an upper bound for the thermodynamic equilibrium between adsorbed water on the surface and droplets of liquid water in the reservoir. Whenever the surface free energy (as plotted at a temperature of 300 K in Fig. 15 for various hydration densities) lies below the surface energy of the clean termination, water adsorption stabilizes the wet surface. Apart from the (010) surface, both (100) and (001) surfaces should be hydrated with water surface densities about 4-5 molecules/nm^2. Furthermore, we point out that the computed surface energy of the wet (001) surface is very close to zero, meaning the energy cost of cleaving the crystal parallel to the (001) orientation could be almost fully compensated by the exothermic process of water adsorption. This prediction holds even when considering dispersion interactions (see Supplementary Materials).

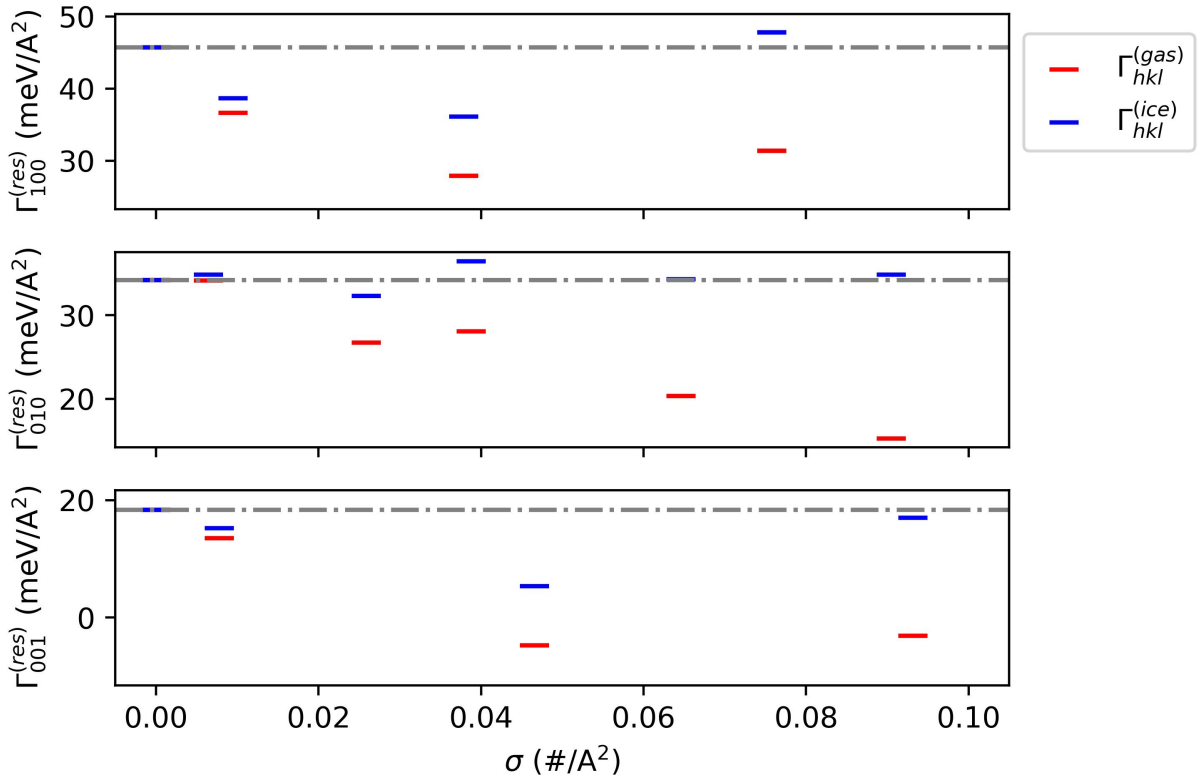

Figure 15: Free surface energy at $T = 300$ K versus the two-dimensional water density (number of water molecules per Å^2). The surface free energy Γ is evaluated either by using the Ice I$_h$ reservoir (blue markers) or the Ideal gas reservoir (red markers) at vapour partial pressure $p = 0.01$ atm. For each surface, the gray dot-dashed line represents the energy of the clean surface. Top panel: the (100) surface; medium panel: the (010) surface; bottom panel: the (001) surface.

Conclusions

The present work focuses on the structure and stability of low-index surfaces of the $Rb_2Ti_2O_5$ perovskite at the atomic scale, either clean or at the onset of water adsorption, by Density Functional Theory calculations.

The unreconstructed clean (100), (010) and (001) surfaces have rather low surface energies, with the latter one being the most stable among the clean terminations. The (1×1) $Rb_2Ti_2O_5$(001) surface has indeed a very low surface energy and moderate surface stress, as compared to other oxide surfaces; the atomic relaxations are limited to the two outermost layers. Our calculations therefore suggest that the clean (1×1) $Rb_2Ti_2O_5$(001) surface is stable against reconstructions. All our findings agree with the fact that the crystal easily cleaves along the (001) planes, consistently with its layered nature. In contrast, the (1×1) (100) clean surface shows a huge tensile surface stress, which is ultimately due to the reduced coordination numbers of the outermost Ti and O ions. We guess that the $Rb_2Ti_2O_5$(100) clean surface could reconstruct and easily react with external molecules.

This is confirmed by the propensity of the (100) surface to react with water. The H_2O molecules spontaneously dissociates; its adsorption is an exothermic process that contributes to stabilize the termination and significantly reduce the surface stress. Hydroxyl groups form at the surface, with chemical bonds that are clearly stronger than the hydrogen bonds in liquid water.

The (001) surface is also very reactive towards water, which adsorbs in its molecular form. The water adsorption enthalpy almost compensates the clean surface energy and the atomic structure of the (001) termination is barely modified by the hydration process, apart from the significant outward relaxation of the Rb atoms. This agrees with the experimental observations of the very high hydrophilic character of the $Rb_2Ti_2O_5$ crystallites. Our calculations indicate that $Rb_2Ti_2O_5$ might spontaneously form quasi two-dimensional hydrated (001) layers of varying thickness when exposed to humid air. The outward Rb relaxation process might ultimately result in the alkali cations solvation in

humid environments, as suggested by the experimental observations of presence of Rb^+ ions at the water overlayers [35].

On the (010) surface water can form interesting symmetric configurations, although this orientation is the less reactive one among the low-index terminations. The water molecules can easily re-orient by crossing low-energy barriers.

Overall, we predict that at ambient conditions the low-index $Rb_2Ti_2O_5$ terminations are covered with water, with a significant two-dimensional surface water density of about 4 molecules/nm^2 on the (100) and (001) surfaces. On these surfaces, the adsorption of water significantly reduces both the surface energy of the clean terminations and the surface stress, which is almost null in the case of the full water monolayer.

All these results point towards a quasi spontaneous exfoliation of the material in presence of water vapour along the (001) surfaces. This renders the study of these surface processes and the subsequent diffusion of charged species on the surface particularly relevant to understand the mechanisms for proton conduction in $Rb_2Ti_2O_5$:$(H_2O)_x$.

Given the high hydrophilic character of $Rb_2Ti_2O_5$, the present study can be followed by an extensive exploration of water-covered surfaces and the processes of ion solvation at the surface and water (or hydroxyl) diffusion into the bulk. This study would likely imply molecular dynamics simulations beyond the ns time-scales and including several hundreds atoms. Scale- and time-limitation that are inherent to DFT-based molecular dynamics simulations could be overcome by constructing interatomic potentials via machine-learning. [40]

Author contributions

F.F. and G.B. designed research, after preliminary work by S.D.S.C.; G.B. carried out the simulations; G.B. and F.F. analyzed data; G.B. made all the graphs; all authors participated in writing the paper.

Conflicts of interest

There are no conflicts to declare.

Data availability

Data for this article, including DFT calculations are available at NOMAD at https://dx.doi.org/10.17172/NOMAD/2024.11.21-1. The most relevant data supporting this article have been included as part of the Supplementary Information.

Acknowledgements

GB acknowledges a PhD fellowship by the Doctoral School ED 397. All authors acknowledge financial support by the French Research National Agency (ANR) via the project MIMETIX (ANR 21 – CE50 – 0035 – 02).

References

[1] H. Iwahara, T. Esaka, H. Uchida, and N. Maeda. Proton conduction in sintered oxides and its application to steam electrolysis for hydrogen production. *Solid State Ionics*, 3/4:359, 1981.

[2] H. Uchida, N. Maeda, and H. Iwahara. Relation between proton and hole conduction in srceo3-based solid electrolytes under water-containing atmospheres at high temperatures. *Solid State Ionics*, 11(2):117, 1983.

[3] H. Iwahara. Proton conducting ceramics and their applications. *Solid State Ionics*, 86(38):9, 1996.

[4] E. C. C. de Souza and R. Muccillo. Properties and applications of perovskite proton conductors. *Mater. Res.*, 13(3):385, 2010.

[5] S. Fop. Solid oxide proton conductors beyond perovskites. *J. Mater. Chem. A*, 9:18836, 2021.

[6] Rémi Federicci, Benoit Baptiste, Fabio Finocchi, Florin Popa, Luc Brohan, Keevin Béneut, Paola Giura, Gwenaëlle Rousse, Armel Descamps-Mandine, Thierry Douillard, Abhay Shukla, and Brigitte Leridon. The crystal structure of $Rb_2Ti_2O_5$. *Acta Cryst. B*, 73(6):1142, 2017.

[7] Rémi Federicci, Stéphane Holé, Aurelian Florin Popa, Luc Brohan, Benoît Baptiste, Silvana Mercone, and Brigitte Leridon. $\mathrm{rb_2ti_2o_5}$: Superionic conductor with colossal dielectric constant. *Phys. Rev. Mater.*, 1:032001.

[8] Rashmi Rani, Sofia De Sousa Coutinho, Stephane Holé, and Brigitte Leridon. Colossal dielectric constant in k2ti2o5. *Materials Letters*, 258:126784, 2020.

[9] Sofia De Sousa Coutinho, Rémi Federicci, Stéphane Holé, and Brigitte Leridon. Virtual cathode induced in rb2ti2o5 solid electrolyte. *Solid State Ionics*, 333:72–75, 2019.

[10] S. Andersson and A.D. Wadsley. Five co-ordinated titanium in k2tio5. *Nature*, 187:499–500, 1960.

[11] S. Andersson and A.D. Wadsley. Alkali metal titanium oxide bronzes. *Nature*, 192:551–552, 1961.

[12] Sofia de Sousa Coutinho, David Bérardan, Guillaume Lang, Rémi Federicci, Paola Giura, Keevin Beneut, Nita Dragoe, Stéphane Holé, and Brigitte Leridon. Effect of water incorporation on the ionic conduction properties of the solid electrolyte material rb2ti2o5.(h2o)x. *Solid State Ionics*, 364:115630, 2021.

[13] Narimane Meziani, Méline Parent, Gwenaëlle Rousse, Brigitte Leridon, David Berardan, and Paola Giura. Chemical and structural evolution of rb2–2xk2xti2o5 layered titanates when exposed to ambient air. *Inorganic Chemistry*, 63(38):17513–17524, 2024. PMID: 39225367.

[14] Seongkoo Kang, Arvinder Singh, Kyle G. Reeves, Jean-Claude Badot, Serge Durand-Vidal, Christophe Legein, Monique Body, Olivier Dubrunfaut, Olaf J. Borkiewicz, Benoît Tremblay, Christel Laberty-Robert, and Damien Dambournet. Hydronium ions stabilized in a titanate-layered structure with high ionic conductivity: Application to aqueous proton batteries. *Chemistry of Materials*, 32(21):9458, 2020.

[15] P Giannozzi, O Andreussi, T Brumme, O Bunau, M Buongiorno Nardelli, M Calandra, R Car, C Cavazzoni, D Ceresoli, M Cococcioni, N Colonna, I Carnimeo, A Dal Corso, S de Gironcoli, P Delugas, R A DiStasio, A Ferretti, A Floris, G Fratesi, G Fugallo, R Gebauer, U Gerstmann, F Giustino, T Gorni, J Jia, M Kawamura, H-Y Ko, A Kokalj, E Küçükbenli, M Lazzeri, M Marsili, N Marzari, F Mauri, N L Nguyen, H-V Nguyen, A Otero de-la Roza, L Paulatto, S Poncé, D Rocca, R Sabatini, B Santra, M Schlipf, A P Seitsonen, A Smogunov, I Timrov, T Thonhauser, P Umari, N Vast, X Wu, and S Baroni. Advanced capabilities for materials modelling with quantum espresso. *Journal of Physics: Condensed Matter*, 29(46):465901, oct 2017.

[16] John P. Perdew, Kieron Burke, and Matthias Ernzerhof. Generalized gradient approximation made simple. *Phys. Rev. Lett.*, 77:3865, Oct 1996.

[17] Yingkai Zhang and Weitao Yang. Comment on "generalized gradient approximation made simple". *Phys. Rev. Lett.*, 80:890, Jan 1998.

[18] D. R. Hamann. Optimized norm-conserving vanderbilt pseudopotentials. *Phys. Rev. B*, 88:085117, Aug 2013.

[19] Stefan Grimme, Jens Antony, Stephan Ehrlich, and Helge Krieg. A consistent and accurate ab initio parametrization of density functional dispersion correction (dft-d) for the 94 elements h-pu. *The Journal of Chemical Physics*, 132(15):154104, 04 2010.

[20] M. Tournoux, R. Marchand, and L. Brohan. Surface energies of solid oxides and carbides. *Prog. Solid State Chem.*, 17:33, 1986.

[21] S.V. Vikram, D.M. Phase, and V.S. Chandel. *J. Mater. Sci. Mater. Electron.*, 21:902, 2010.

[22] A. Kokalj. Computer graphics and graphical user interfaces as tools in simulations of matter at the atomic scale. *Comp. Mater. Sci.*, 28:155, 2003.

[23] R.J. Needs, M.J. Godfrey, and M. Mansfield. Theory of surface stress and surface reconstruction. *Surface Science*, 242(1):215, 1991.

[24] Pierre Müller, Andres Saùl, and Frédéric Leroy. Simple views on surface stress and surface energy concepts. *Advances in Natural Sciences: Nanoscience and Nanotechnology*, 5(1):013002, nov 2013.

[25] K. Reuter and M. Scheffler. *Phys. Rev. B*, 65:035406, 2001.

[26] A Glassner. The thermochemical properties of the oxides, fluorides, and chlorides to 2500 k. *Argonne Nat.Lab. Reports*, ANL-5750:1–72, 1956.

[27] L. Pauling. The structure and entropy of ice and of other crystals with some randomness of atomic arrangement. *J. Am. Chem. Soc.*, 57:2680, 1935.

[28] N. H. Fletcher. *The Chemical Physics of Ice*. Cambridge University Press, 1970.

[29] F. Finocchi and J. Goniakowski. The effects of exchange and correlation on the computed equilibrium shapes of wet mgo crystallites. *Surface Science*, 601(18):4144, 2007.

[30] Yoyo Hinuma, Yu Kumagai, Fumiyasu Oba, and Isao Tanaka. Categorization of surface polarity from a crystallographic approach. *Computational Materials Science*, 113:221, 2016.

[31] P. W. Tasker. The stability of ionic crystal surfaces. *J. Phys. C: Solid State Phys.*, 12:4977, 1979.

[32] J. Goniakowski, F. Finocchi, and C. Noguera. Polarity of oxide surfaces and nanostructures. *Reports Prog. Phys.*, 71(1):0165011, 2007.

[33] D.T. Livey and P. Murray. Surface energies of solid oxides and carbides. *J. Amer. Ceramic Soc.*, 39(11):363, 1956.

[34] S. Yasumura, T. Kamashi, T. Toyao, K. Shimizu, and Y. Hinuma. Prediction of stable surfaces of metal oxides through the unsaturated coordination index. *ACS Omega*, 8:29779, 2023.

[35] Valerio Digiorgio, Karen Sobnath, Maria Luisa Della Rocca, Clément Barraud, Rémi Federicci, Armel Descamps-Mandine, and Brigitte Leridon. Rb2ti2o5: A layered ionic conductor at the sub-micrometer scale. *Applied Physics Letters*, 126(1):013506, 01 2025.

[36] Michele Lazzeri and Annabella Selloni. Stress-driven reconstruction of an oxide surface: The anatase $\mathrm{tio}_2(001) - (1 \times 4)$ surface. *Phys. Rev. Lett.*, 87:266105, Dec 2001.

[37] Fabio Pietrucci. Strategies for the exploration of free energy landscapes: Unity in diversity and challenges ahead. *Reviews in Physics*, 2:32, 2017.

[38] F. Finocchi, R. Hacquart, C. Naud, and J. Jupille. Hydroxyl-defect complexes on hydrated mgo smokes. *The Journal of Physical Chemistry C*, 112(34):13226, 2008.

[39] Fabio Finocchi, Pascale Geysermans, and Antonin Bourgeois. The role of hydroxylation in the step stability and in the interaction between steps: a first-principles study of vicinal mgo surfaces. *Phys. Chem. Chem. Phys.*, 14:13692, 2012.

[40] Venkat Kapil, Dávid Péter Kovács, Gábor Csányi, and Angelos Michaelides. First-principles spectroscopy of aqueous interfaces using machine-learned electronic and quantum nuclear effects. *Faraday Discuss.*, 249:50–68, 2024.